actuators

MDPI

Article

Finite-Time Fault-Tolerant Attitude Control for Quadrotor via Adaptive Sliding Mode Control and RBFNN Observer

Dun Ao, Chiyu Zhang and Fei Lei *

School of Information Science and Technology, Beijing University of Technology, Beijing 100124, China; aodun@bjut.edu.cn (D.A.)
* Correspondence: leifei@bjut.edu.cn

Abstract

This paper presents an observer-assisted barrier adaptive sliding mode controller for quadrotor attitude tracking under nonlinear uncertainties, external disturbances, and matched actuator faults. An RBFNN observer estimates the nominal nonlinear dynamics and disturbances using linear and fractional-power error feedback, whereas the barrier term compensates for the remaining estimation residual and fault effect. An initial-error compensation term initializes the sliding variable at zero. Under bounded-fault and neural-approximation assumptions, Lyapunov analysis establishes bounded neural weights, finite-time entry of the observer error into an explicit neighborhood, forward invariance of the prescribed sliding domain, and bounds on the barrier gain and attitude-tracking error. Comparative simulations against a published fault-tolerant controller, together with combined-stress tests and mechanism-specific ablations, show improved post-fault tracking with the simulated control torques remaining within the prescribed limits and verify the respective roles of the modified sliding surface and observer compensation.

Keywords: adaptive sliding mode control; barrier function; finite-time stability; neural network; quadrotor

1. Introduction

In recent years, quadrotor UAVs have attracted growing research interest due to their extensive applications in agricultural production, data acquisition, logistics delivery, and other fields [1]. Compared with traditional aircraft, quadrotor UAVs offer notable advantages such as light weight, simple mechanical structure, excellent maneuverability, and vertical take-off and landing capabilities [2,3]. Nevertheless, the quadrotor UAV is an underactuated, highly coupled, and strongly nonlinear system [4,5]. During actual flight missions, it is inevitably subject to model uncertainties, external environmental disturbances, and actuator faults [6,7]. Faults of UAVs will degrade the performance and even cause mission failure; due to the requirements of high maneuverability and high real-time response of quadrotor UAVs, fault-tolerant control of UAVs is usually combined with the finite-time stability theory [8,9], so it is particularly important to design finite-time fault-tolerant control for quadrotor UAVs.

The SMC scheme has attracted extensive attention due to its excellent robustness. Hence, it has been widely adopted in many fields, including robotic control, motor control, and power control [10–12]. Sliding mode control (SMC) is distinguished by its inherent disturbance rejection capabilities against nonlinear structures, unmodeled dynamics, and external perturbations, making it fairly effective in maintaining the stability of quadrotors

Check for updates

Academic Editor: Zhenghua Chen

Received: 12 October 2026
Revised: 6 November 2026
Accepted: 16 November 2026
Published: 17 November 2026

Copyright: © 2026 by the authors. Licensee MDPI, Basel, Switzerland. This article is an open access article distributed under the terms and conditions of the Creative Commons Attribution (CC BY) license.

across various operating conditions [13]. The relatively straightforward design of SMC further facilitates its implementation in complex UAV dynamics [14]. To enhance the disturbance rejection capability of the system, a sufficiently large fixed switching gain has been employed in traditional SMC to account for the maximum possible magnitude of model uncertainties and external perturbations [15]. However, the accuracy of the aforementioned controllers heavily relies on precise knowledge of the system model and parameters. Furthermore, their control performance tends to degrade under parameter variations induced by load changes, and they typically require prior knowledge of the upper bounds for both model uncertainties and external disturbances.

To effectively handle the aforementioned model uncertainties and external disturbances, various adaptive control techniques have been widely investigated. The authors of [16] proposed an adaptive terminal sliding mode tracking control method with fast arrival conditions to realize the synchronization of chaotic systems at the transceiver in a limited time. A synthesized adaptive SMC strategy is presented in Reference [17] to cope with abrupt and external disturbances. The authors of [18] proposed an adaptive super-twisting nonsingular fast terminal sliding mode method to overcome the problems of system uncertainties and external disturbances in a 2-DOF helicopter system. Nevertheless, the ultimate bound of the convergence error in such methods is inherently tied to the magnitude of the disturbance, which is typically unmeasurable and hard to estimate in advance. To address this, barrier functions are introduced as smooth mathematical formulations defined within a restricted open neighborhood of the origin [19]. As the system variable drifts toward the predefined boundaries, the barrier function's value grows toward infinity, which significantly improves the problems of overestimation and the chattering of the control signal. Furthermore, the authors of [20] designed a barrier function-based sliding mode controller, which incorporates a modified sliding surface to eliminate the reaching phase, thereby effectively mitigating the chattering phenomenon.

Observer-based sliding mode control has become an important research direction for quadrotor attitude regulation because it can reconstruct lumped disturbances online and alleviate the conservatism of large switching gains. An adaptive disturbance observer combined with fast nonsingular terminal sliding mode control has been shown to improve both disturbance estimation and finite-time tracking performance for quadrotors [21]. An extended-state-observer-assisted integral sliding mode controller has also been reported for nonlinear quadrotor systems, where the observer estimates model uncertainties and external disturbances to enhance robustness [22]. For high-order helicopter systems with model uncertainties and unknown disturbances, a learning observer-based sliding mode control framework was developed by decomposing the plant into coupled subsystems and designing improved learning observers for real-time disturbance estimation, which demonstrates the effectiveness of observer learning in handling high-order dynamics and multi-source disturbances [23]. For quadrotor attitude control with actuator dynamics, a high-order sliding mode disturbance observer was introduced to estimate matched and unmatched disturbances as well as their high-order derivatives in finite time, thereby improving tracking accuracy under nonlinear couplings, model uncertainties, and external perturbations [24]. To further enhance convergence performance under inertia uncertainties, external disturbances, and actuator faults, a prescribed-time unknown input observer was constructed to estimate lumped disturbances without requiring prior knowledge of their upper bounds, and the estimated values were fed back into the attitude controller to achieve prescribed-time tracking [25]. In addition, neural-network-based disturbance observers have been combined with prescribed-performance sliding mode control to estimate unknown disturbances online, showing that observer compensation can be integrated with performance-constrained sliding surfaces to improve robustness

and transient behavior [26]. For nonlinear systems subject to actuator failures, an RBFNN observer has also been incorporated with super-twisting sliding mode control, where the observer improves uncertainty and fault estimation while the fixed-time controller enhances convergence speed and active fault-tolerant capability [27].

Recent learning-based control studies have also extended finite- and fixed-time methods to constrained guidance, attitude regulation, and cooperative systems. A finite-time critic-learning mechanism was developed for optimal elliptical encircling of UAVs under prescribed constraints [28], while an enhanced fixed-time guidance scheme combined uncertainty estimation with collision-free multi-UAV coordination [29]. For hypersonic morphing vehicles, a coordinate transformation and critic-only learning were used to obtain adaptive attitude control without recursive backstepping [30]. Concurrent learning has also been incorporated into adaptive-critic formation control to improve weight convergence while accounting for multirobot safety constraints [31]. These studies demonstrate the benefits of convergence-assured learning and explicit constraint handling; however, their main objectives differ from matched-fault attenuation in a quadrotor attitude loop. The present work instead integrates online uncertainty compensation with a barrier-based residual-robust term and a modified global sliding surface.

Motivated by the above considerations, this paper develops an observer-assisted barrier adaptive sliding mode controller for quadrotor attitude tracking. The design combines online compensation of nominal uncertainties with robust feedback acting on the remaining compensation residual and matched actuator faults. The main contributions are summarized as follows:

- An RBFNN-observer-assisted barrier adaptive control scheme is developed for uncertain quadrotor attitude dynamics with actuator faults. The observer targets the nominal nonlinear dynamics and external disturbances, and the resulting compensation is incorporated into the control input so that the barrier term acts on the remaining compensation residual and fault effect. An initial-error compensation term initializes the modified sliding variable at zero, placing the initial state inside the prescribed barrier domain.
- A quantitative closed-loop analysis connects the observer bounds to the barrier-domain and attitude-tracking guarantees. Lyapunov estimates characterize a practical finite-time neighborhood for the observer error, together with bounds on the neural weights. These estimates yield an explicit bound on the residual entering the sliding dynamics, from which forward invariance of the prescribed sliding domain, bounded barrier gains, and finite-time entry into enlarged tracking-error neighborhoods are established. The analysis makes the dependence of the certified bounds on the observer parameters and fault magnitude explicit.
- A comparative simulation study is conducted using a published fault-tolerant benchmark, a combined-stress condition, and mechanism-specific ablations. Under common plant, reference, fault, and torque constraints, the results demonstrate the post-fault tracking performance of the proposed controller and identify the respective contributions of the modified sliding surface and observer compensation.

2. Preliminaries

Throughout the paper, the following mathematical lemmas and definitions are utilized for the stability analysis of the proposed control scheme. The control system structure is illustrated in Figure 1.

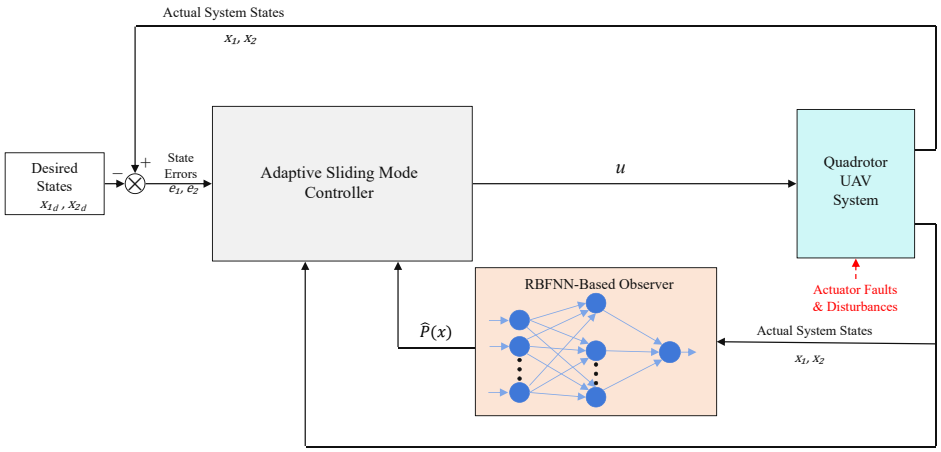


Figure 1. Control system structure diagram.

Lemma 1 ([32,33]). *For any real numbers $x_i \geq 0$ $(i = 1, \ldots, n)$ and real constant $0 < \alpha < 1$, the following inequality holds:*

$$\left(\sum_{i=1}^{n} x_i\right)^{\alpha} \leq \sum_{i=1}^{n} x_i^{\alpha}. \tag{1}$$

Lemma 2 ([34] (Young's Inequality)). *For any real matrices $A, B \in \mathbb{R}^{m \times n}$, the following inequality regarding the matrix trace and Frobenius norm holds:*

$$\mathrm{tr}(A^T B) \leq \frac{1}{2}\|A\|_F^2 + \frac{1}{2}\|B\|_F^2. \tag{2}$$

Lemma 3 ([35,36]). *For any real variable $x \geq 0$ and constant $0 < \alpha < 1$, the following inequality is satisfied:*

$$x^{\alpha} - x \leq (1 - \alpha)\alpha^{\frac{\alpha}{1-\alpha}}. \tag{3}$$

Lemma 4 (Practical Finite-Time Stability). *Let V be a continuous, positive-definite, proper function that is absolutely continuous along the considered trajectories. Suppose that, for constants $\kappa > 0$, $0 < \alpha < 1$, and $C > 0$,*

$$\dot{V} \leq -\kappa V^{\alpha} + C \tag{4}$$

holds almost everywhere. For any $0 < \vartheta < 1$, the trajectory enters the compact sublevel set

$$\left\{ V \leq \left(\frac{C}{(1-\vartheta)\kappa}\right)^{1/\alpha} \right\}$$

in finite time and remains in that set.

Remark 1. *In the stability analysis involving neural networks, the Frobenius norm of a matrix A is defined as $\|A\|_F = \sqrt{\mathrm{tr}(A^T A)}$. This property is frequently used to transform multi-dimensional weight errors into a scalar equivalent for rigorous stability proofs.*

3. Problem Formulation

To formulate the control problem, we consider the rigid-body kinematics and rotational dynamics.

Let $\boldsymbol{\xi} = [\phi, \theta, \psi]^T$ denote the roll, pitch, and yaw angles under the Z–Y–X Euler-angle convention, and let $\boldsymbol{\omega} = [p, q, r]^T$ denote the body-frame angular velocity. Their exact kinematic relationship is

$$\dot{\boldsymbol{\xi}} = T(\phi, \theta)\boldsymbol{\omega}, \qquad T(\phi, \theta) = \begin{bmatrix} 1 & \sin\phi\tan\theta & \cos\phi\tan\theta \\ 0 & \cos\phi & -\sin\phi \\ 0 & \sin\phi\sec\theta & \cos\phi\sec\theta \end{bmatrix}, \tag{5}$$

which is nonsingular provided that $\cos\theta \neq 0$.

Assumption 1 (Kinematic operating domain). *The quadrotor is modeled as a rigid body whose body axes coincide with its principal inertia axes, so that the inertia matrix is diagonal. The considered attitude trajectories remain in a compact nonsingular operating set satisfying* $|\phi| \leq \bar{\phi}$, $|\theta| \leq \bar{\theta} < \pi/2$, $\|\boldsymbol{\omega}\| \leq \bar{\omega}$, *and* $\|\dot{\boldsymbol{\omega}}\| \leq \bar{a}_{\omega}$. *The controller is developed for near-hover and moderate-attitude operation, for which* $T(\phi, \theta) \approx I_3$ *and hence* $[\dot{\phi}, \dot{\theta}, \dot{\psi}]^T \approx [p, q, r]^T$. *Translational dynamics are not included explicitly in the attitude-loop model, while bounded residual aerodynamic and rotor-coupling effects entering the rotational dynamics are represented by the lumped uncertainty and disturbance terms.*

Under Assumption 1, the approximate kinematics and rigid-body rotational dynamics used for controller design are written as

$$\begin{cases} \dot{\phi} = p \\ \dot{\theta} = q \\ \dot{\psi} = r \\ \dot{p} = \dfrac{I_y - I_z}{I_x} qr + \dfrac{u_1}{I_x} + \dfrac{d_1}{I_x} \\ \dot{q} = \dfrac{I_z - I_x}{I_y} pr + \dfrac{u_2}{I_y} + \dfrac{d_2}{I_y} \\ \dot{r} = \dfrac{I_x - I_y}{I_z} pq + \dfrac{u_3}{I_z} + \dfrac{d_3}{I_z} \end{cases} \tag{6}$$

In the above model, ϕ, θ, and ψ stand for the Euler angles, while p, q, and r denote the body-frame angular velocities. The constants I_x, I_y, and I_z are the moments of inertia. Furthermore, the terms u_i and d_i correspond to the control inputs and external disturbances, respectively.

The kinematic approximation error can be written as

$$\boldsymbol{\Delta}_{\text{kin}} = \big[T(\phi, \theta) - I_3\big]\boldsymbol{\omega}. \tag{7}$$

On the compact operating set in Assumption 1, it satisfies $\|\boldsymbol{\Delta}_{\text{kin}}\| \leq \bar{\delta}_T \bar{\omega}$, where $\bar{\delta}_T = \sup_{|\phi| \leq \bar{\phi}, |\theta| \leq \bar{\theta}} \|T(\phi, \theta) - I_3\| < \infty$. The corresponding bounded terms in the second-order attitude model are included in the lumped nonlinear function estimated by the RBFNN observer. Therefore, the proposed control strategy applies to attitude tracking on the stated compact, nonsingular operating domain.

For the convenience of subsequent control design, it is common practice to rewrite the detailed physical model into a compact second-order nonlinear form:

$$\begin{cases} \dot{x}_1 = x_2 \\ \dot{x}_2 = F(x) + b(u + \rho(x, t)) + d \end{cases} \tag{8}$$

Here, $x_1 = \boldsymbol{\xi}$ and $x_2 = \dot{\boldsymbol{\xi}} \approx \boldsymbol{\omega}$ under Assumption 1, while $b = \mathrm{diag}(1/I_x, 1/I_y, 1/I_z)$. The function $F(x)$ contains the nominal rotational coupling terms together with bounded modeling terms, and d denotes the transformed external disturbance. Since the exact system dynamics are usually unavailable in practice, we employ a neural network observer for online estimation. The dynamic equation of the state estimator is constructed as follows:

$$\dot{\hat{x}}_2 = \hat{W}^T h(x) + bu + \hat{\varepsilon}\,\mathrm{sign}(e_2') + Le_2' + \beta(e_2')^{\frac{p}{q}} \tag{9}$$

Let the desired attitude trajectory x_{1d} be twice continuously differentiable, with x_{1d}, $\dot{x}_{1d}$, and $\ddot{x}_{1d}$ bounded. Set $x_{2d} = \dot{x}_{1d}$. The tracking errors are defined as:

$$\begin{cases} e_1 &= x_1 - x_{1d} \\ e_2 &= x_2 - x_{2d} \end{cases} \tag{10}$$

Consequently, $\dot{e}_1 = e_2$.

Simultaneously, the estimation error of the observer is defined as:

$$e_2' = x_2 - \hat{x}_2 \tag{11}$$

4. Main Works

4.1. Finite-Time Control Framework

To improve control performance, we define the sliding surface as:

$$\begin{cases} s = \bar{s} - s_c \\ \bar{s} = ce_1 + e_2 \end{cases} \tag{12}$$

where $s_c(t) = \bar{s}(0)e^{-\gamma t}$, with $c > 0$ and $\gamma > 0$ being design control parameters satisfying $c \neq \gamma$. Here, $\bar{s}(0) = ce_1(0) + e_2(0)$ is the initial value of $\bar{s}$ and is held constant in $s_c(t)$. Consequently, $s_c(0) = \bar{s}(0)$ and $s(0) = 0$.

The observer is designed with the nominal nonlinear dynamics and external disturbance as its estimation target, denoted by $P(x) = F(x) + d$. Explicit time dependence in P is suppressed for brevity. On a prescribed operating domain $\mathcal{X}$, assume the representation

$$P(x) = W^{*T} h(x) + \varepsilon(x, t), \tag{13}$$

where $h(x) \in \mathbb{R}^m$, $W^* \in \mathbb{R}^{m\times 3}$ is a constant ideal weight matrix, and $\hat{W} \in \mathbb{R}^{m\times 3}$ is its estimate. The basis functions and approximation residual satisfy $\|h(x)\|_2 \leq \bar{h}$ and $\|\varepsilon(x,t)\|_\infty \leq \bar{\varepsilon}$ uniformly on $\mathcal{X}$, with finite constants $\bar{h}$ and $\bar{\varepsilon}$. The following analysis is stated for trajectories on which these approximation bounds hold.

The observer output combines the neural approximation with linear and fractional-power error feedback:

$$\hat{P}(x) = \hat{W}^T h(x) + \hat{\varepsilon}\,\mathrm{sign}(e_2') + Le_2' + \beta(e_2')^{\ell_1/\ell_2}. \tag{14}$$

Here, $\hat{\varepsilon} \geq \bar{\varepsilon}$, $L > 0$, and $\beta > 0$; ℓ_1 and ℓ_2 are positive odd integers satisfying $\ell_1 < \ell_2$. Let $\nu = \ell_1/\ell_2 \in (0,1)$. Fractional powers are applied componentwise, so that $(e_{2i}')^\nu = |e_{2i}'|^\nu \,\mathrm{sign}(e_{2i}')$. The discontinuous observer dynamics are considered in the Filippov sense, with the set-valued signum map satisfying $\mathrm{Sgn}(0) = [-1, 1]$ componentwise. The differential inequalities below hold for almost every time along absolutely continuous solutions. The fractional-power feedback is defined to be zero when its argument is zero.

Based on the neural network estimation, the overall control law is designed as:

$$u = b^{-1}\left[\dot{x}_{2d} - \hat{P}(x) - ce_2 - \gamma s_c - \boldsymbol{k}\,\mathrm{sign}(s)\right] \tag{15}$$

where $\boldsymbol{k} = \mathrm{diag}(k_1, k_2, k_3)$ denotes the robust adaptive gain matrix. The barrier gain of each attitude channel ($i = 1, 2, 3$) is computed from the sliding variable and the design parameters to compensate for the residual uncertainty:

$$k_i = \frac{\eta |s_i|}{\sigma - |s_i|} \tag{16}$$

Here, $\eta > 0$ sets the gain scale and $\sigma > 0$ defines the open domain $|s_i| < \sigma$. The gain is singular at the boundary of this domain. Admissibility of the trajectories and the resulting gain bounds are established in Proposition 2.

4.2. Observer Convergence Analysis

Assume that the matched fault satisfies $\|b\rho(x,t)\|_2 \le \rho_M$ uniformly along the considered trajectories, where $\rho_M \ge 0$ is finite. Define $\tilde{W} = W^* - \hat{W}$ and

$$V_0 = V_{0,e} + V_{0,w}, \qquad V_{0,e} = \frac{1}{2}\|e_2'\|_2^2, \qquad V_{0,w} = \frac{1}{2\lambda}\|\tilde{W}\|_F^2. \tag{17}$$

The weight update law is

$$\dot{\hat{W}} = \lambda\left(h(x)e_2'^T - \sigma_w \hat{W}\right), \tag{18}$$

where $\lambda > 0$ is the learning gain and $\sigma_w > 0$ is the leakage coefficient.

Proposition 1 (Observer error bounds)**.** *Suppose that the approximation and fault bounds stated above hold, and that $\hat{\varepsilon} \ge \bar{\varepsilon}$, $L > 0$, $\beta > 0$, $\lambda > 0$, and $\sigma_w > 0$. Define*

$$\begin{aligned} \alpha &= \frac{\ell_1 + \ell_2}{2\ell_2} \in (0,1), \qquad \Delta_0 = (1-\alpha)\alpha^{\alpha/(1-\alpha)}, \\ \kappa &= \min\{2^\alpha \beta, \sigma_w \lambda\}, \\ C_L &= \sigma_w \lambda \Delta_0 + \frac{\sigma_w}{2}\|W^*\|_F^2 + \frac{\rho_M^2}{2L}. \end{aligned} \tag{19}$$

For any $0 < \vartheta < 1$, let

$$\mathcal{V}_\vartheta = \left(\frac{C_L}{(1-\vartheta)\kappa}\right)^{1/\alpha}, \qquad \bar{V}_0 = \max\{V_0(0), \mathcal{V}_\vartheta\}. \tag{20}$$

Then $V_0(t) \le \bar{V}_0$ for all $t \ge 0$. The sublevel set $V_0 \le \mathcal{V}_\vartheta$ is reached at an entrance time T_o satisfying

$$T_o \le \frac{\max\{V_0(0)^{1-\alpha} - \mathcal{V}_\vartheta^{1-\alpha}, 0\}}{\vartheta\kappa(1-\alpha)}. \tag{21}$$

For all $t \ge T_o$,

$$\|e_2'(t)\|_2 \le \sqrt{2\mathcal{V}_\vartheta}, \qquad \|\tilde{W}(t)\|_F \le \sqrt{2\lambda\mathcal{V}_\vartheta}. \tag{22}$$

Proof. Equations (9) and (13) give

$$\begin{aligned} \dot{e}_2' = {} & \tilde{W}^T h(x) + \varepsilon + b\rho - \hat{\varepsilon}\,\mathrm{sign}(e_2') \\ & - Le_2' - \beta(e_2')^\nu. \end{aligned} \tag{23}$$

Since W^* is constant, $\dot{\tilde{W}} = -\dot{\hat{W}}$. The identity

$$e_2'^T \tilde{W}^T h(x) = \operatorname{tr}\big(\tilde{W}^T h(x) e_2'^T\big)$$

cancels the neural cross term in the derivative of (17), yielding

$$\begin{aligned} \dot{V}_0 = {} & e_2'^T \varepsilon - \hat{\varepsilon}\|e_2'\|_1 - L\|e_2'\|_2^2 - \beta \sum_{i=1}^{3} |e_{2i}'|^{1+\nu} \\ & + e_2'^T b\rho + \sigma_w \operatorname{tr}(\tilde{W}^T \hat{W}). \end{aligned} \tag{24}$$

The approximation-error terms satisfy

$$e_2'^T \varepsilon - \hat{\varepsilon}\|e_2'\|_1 \le (\bar{\varepsilon} - \hat{\varepsilon})\|e_2'\|_1 \le 0.$$

For every $L > 0$, Young's inequality gives

$$e_2'^T b\rho \le \rho_M \|e_2'\|_2 \le \frac{L}{2}\|e_2'\|_2^2 + \frac{\rho_M^2}{2L}. \tag{25}$$

The leakage term satisfies

$$\begin{aligned} \sigma_w \operatorname{tr}(\tilde{W}^T \hat{W}) &= \sigma_w \operatorname{tr}(\tilde{W}^T W^*) - \sigma_w \|\tilde{W}\|_F^2 \\ &\le -\frac{\sigma_w}{2}\|\tilde{W}\|_F^2 + \frac{\sigma_w}{2}\|W^*\|_F^2 \\ &= -\sigma_w \lambda V_{0,w} + \frac{\sigma_w}{2}\|W^*\|_F^2. \end{aligned} \tag{26}$$

By Lemma 1,

$$\sum_{i=1}^{3} |e_{2i}'|^{1+\nu} = \sum_{i=1}^{3} \big(|e_{2i}'|^2\big)^{\alpha} \ge \|e_2'\|_2^{2\alpha} = 2^{\alpha} V_{0,e}^{\alpha}.$$

Consequently,

$$\begin{aligned} \dot{V}_0 \le {} & -L V_{0,e} - 2^{\alpha}\beta V_{0,e}^{\alpha} - \sigma_w \lambda V_{0,w} \\ & + \frac{\sigma_w}{2}\|W^*\|_F^2 + \frac{\rho_M^2}{2L}. \end{aligned} \tag{27}$$

Lemma 3 yields

$$-\sigma_w \lambda V_{0,w} \le -\sigma_w \lambda V_{0,w}^{\alpha} + \sigma_w \lambda \Delta_0.$$

Using (19) and Lemma 1, it follows that

$$\begin{aligned} \dot{V}_0 &\le -L V_{0,e} - \kappa\big(V_{0,e}^{\alpha} + V_{0,w}^{\alpha}\big) + C_L \\ &\le -\kappa V_0^{\alpha} + C_L. \end{aligned} \tag{28}$$

Whenever $V_0 \ge \mathcal{V}_{\vartheta}$,

$$\dot{V}_0 \le -\vartheta \kappa V_0^{\alpha}.$$

Integration up to the first entrance into $V_0 \le \mathcal{V}_{\vartheta}$ gives (21). At the boundary, the same inequality is strictly negative, so an outward crossing is excluded by the integral comparison argument. This establishes invariance of the sublevel set, the uniform estimate $V_0(t) \le \bar{V}_0$, and the component bounds (22). □

The weight dynamics also admit a separate bound. Define the uniform observer estimates

$$E_o = \sqrt{2\bar{V}_0}, \qquad W_o = \sqrt{2\lambda \bar{V}_0}, \tag{29}$$

so that $\|e_2'(t)\|_2 \le E_o$ and $\|\tilde{W}(t)\|_F \le W_o$ for all $t \ge 0$. Integration of (18) gives

$$\hat{W}(t) = e^{-\lambda\sigma_w t}\hat{W}(0) + \lambda \int_0^t e^{-\lambda\sigma_w(t-\tau)} h(x(\tau)) e_2'(\tau)^T \, d\tau.$$

Since $\|h(x)e_2'^T\|_F = \|h(x)\|_2 \|e_2'\|_2$, one obtains

$$\begin{aligned} \|\hat{W}(t)\|_F \le{}& e^{-\lambda\sigma_w t}\|\hat{W}(0)\|_F \\ &+ \frac{\bar{h}E_o}{\sigma_w}\left(1 - e^{-\lambda\sigma_w t}\right). \end{aligned} \tag{30}$$

Thus, the leakage coefficient bounds the sustained response of the weight dynamics to the adaptation signal, while $\lambda\sigma_w$ determines the decay rate of their initial condition contribution.

Remark 2. *The linear and fractional-power feedback terms act on different error scales. For a nonzero scalar error magnitude r, the ratio of their magnitudes is $\beta r^{\nu-1}/L$. The fractional-power contribution therefore becomes relatively stronger as the error decreases, whereas the linear term contributes quadratic damping in* (27)*. The latter also absorbs the fault cross term through* (25)*. The resulting estimate applies for every $L > 0$; the fault contribution to C_L increases as L decreases.*

Remark 3. *The condition $\hat{\varepsilon} \ge \bar{\varepsilon}$ requires an available upper bound on the neural approximation residual over the operating domain. The constants ρ_M and $\|W^*\|_F$ enter the performance bounds, but are not used in the online evaluation of the observer or the control law. Numerical certification of* (20) *requires estimates of these constants and of the initial observer energy. The barrier gain* (16) *is evaluated without supplying the fault bound or the bound on the residual remaining after observer compensation.*

4.3. Closed-Loop Stability Analysis

The uniform observer estimates are used to bound the residual entering the sliding dynamics. From $\dot{e}_1 = e_2$ and $\dot{s}_c = -\gamma s_c$, differentiation of the sliding variable gives:

$$\begin{aligned} \dot{s} &= \dot{\tilde{s}} - \dot{s}_c = c\dot{e}_1 + \dot{e}_2 + \gamma s_c \\ &= c\dot{e}_1 + P(x) + b(u + \rho(x,t)) - \dot{x}_{2d} + \gamma s_c \end{aligned} \tag{31}$$

Substitution of (15) gives the residual

$$\begin{aligned} \mathbf{\Pi} &= P - \hat{P} + b\rho \\ &= \tilde{W}^T h(x) + \varepsilon + b\rho - \hat{\varepsilon}\,\mathrm{sign}(e_2') - Le_2' - \beta(e_2')^{\nu}. \end{aligned}$$

Using (29), its components satisfy

$$\begin{aligned} \|\mathbf{\Pi}(t)\|_\infty &\le \bar{h}\|\tilde{W}(t)\|_F + \bar{\varepsilon} + \rho_M + \hat{\varepsilon} \\ &\quad + L\|e_2'(t)\|_2 + \beta\|e_2'(t)\|_2^{\nu} \\ &\le \bar{h}W_o + \bar{\varepsilon} + \rho_M + \hat{\varepsilon} + LE_o + \beta E_o^{\nu} =: \Xi. \end{aligned}$$

This estimate holds from the initial time under the stated approximation and fault assumptions. The constant Ξ is used for analysis and is not an input to the barrier gain. The sliding dynamics are

$$\begin{aligned} \dot{\boldsymbol{s}} &= P(x) - \hat{P}(x) + b\rho(x,t) - \boldsymbol{k}\,\mathrm{sign}(\boldsymbol{s}) \\ &= -\boldsymbol{k}\,\mathrm{sign}(\boldsymbol{s}) + \mathbf{\Pi} \end{aligned} \tag{32}$$

Define the auxiliary residual radius

$$r_b = \sigma\left(\frac{\Xi}{\Xi+\eta}\right). \tag{33}$$

Since $\eta > 0$ and $\Xi \geq 0$, one has $0 \leq r_b < \sigma$.

Proposition 2 (Forward invariance of the barrier domain)**.** *Consider the sliding dynamics* (32) *with the gain* (16)*, where* $\eta > 0$*,* $\sigma > 0$*, and the measurable residual satisfies* $\|\mathbf{\Pi}(t)\|_\infty \leq \Xi$ *almost everywhere. Let* r_b *be defined by* (33)*, and assume that* $|s_i(0)| < \sigma$ *for* $i = 1, 2, 3$*. Define*

$$R_i = \max\{|s_i(0)|, r_b\} < \sigma.$$

Then the set $\mathcal{D}_\sigma = \{\boldsymbol{s} \in \mathbb{R}^3 : |s_i| < \sigma,\ i = 1, 2, 3\}$ *is forward invariant. In particular, for all* $t \geq 0$*,*

$$|s_i(t)| \leq R_i, \qquad \sigma - |s_i(t)| \geq \sigma - R_i > 0, \qquad 0 \leq k_i(t) \leq \frac{\eta R_i}{\sigma - R_i}.$$

Proof. Within $\mathcal{D}_\sigma$, the identity

$$k_i \operatorname{sign}(s_i) = \frac{\eta s_i}{\sigma - |s_i|}$$

holds, including at $s_i = 0$. The map on the right-hand side is locally Lipschitz in s_i. Hence, for each bounded measurable residual, the sliding dynamics admit a unique maximal absolutely continuous solution in $\mathcal{D}_\sigma$. Denote its maximal existence time by $T_{\max}$.

Let $r_i(t) = |s_i(t)|$. For almost every $t \in [0, T_{\max})$ such that $r_i(t) > 0$,

$$\begin{aligned}
\dot{r}_i &= \operatorname{sign}(s_i)\dot{s}_i \\
&= -\frac{\eta r_i}{\sigma - r_i} + \operatorname{sign}(s_i)\Pi_i \\
&\leq \Xi - \frac{\eta r_i}{\sigma - r_i} \\
&= -\frac{(\Xi+\eta)(r_i - r_b)}{\sigma - r_i}.
\end{aligned}$$

For any $r_* \in (R_i, \sigma)$, one has $r_* > r_b$ and $r_i(0) < r_*$. Whenever $r_* \leq r_i(t) < \sigma$, the monotonicity of $\eta r/(\sigma - r)$ gives

$$\dot{r}_i(t) \leq \Xi - \frac{\eta r_*}{\sigma - r_*} = -\frac{(\Xi+\eta)(r_* - r_b)}{\sigma - r_*} < 0 \quad \text{almost everywhere.}$$

Suppose that $r_i(t) > r_*$ for some $t < T_{\max}$. Since $r_i(0) < r_*$, continuity provides an interval (t_a, t_b) on which $r_i(t) > r_*$ with $r_i(t_a) = r_*$. Integrating the preceding strictly negative bound from t_a to any $t \in (t_a, t_b)$ yields $r_i(t) < r_*$, a contradiction. Therefore, $r_i(t) \leq r_*$ for $0 \leq t < T_{\max}$. Since r_* can be chosen arbitrarily close to R_i from above, it follows that $r_i(t) \leq R_i$.

The resulting bound confines $\boldsymbol{s}(t)$ to a compact subset of $\mathcal{D}_\sigma$. Together with the bounded residual and local Lipschitz property, this excludes a finite escape time for the sliding dynamics and yields $T_{\max} = \infty$. The positive denominator margin follows directly, and the gain bound follows from the monotonicity of $\eta r/(\sigma - r)$. □

For the prescribed initialization $s_c(0) = \bar{s}(0)$, one has $s(0) = 0$ and $R_i = r_b$. Consequently,

$$|s_i(t)| \leq r_b < \sigma, \qquad \sigma - |s_i(t)| \geq \frac{\sigma\eta}{\Xi+\eta} > 0, \qquad 0 \leq k_i(t) \leq \Xi, \qquad t \geq 0.$$

Thus, every $\sigma > 0$ satisfies the initial admissibility condition under exact initialization. If an initialization error is present, σ must instead satisfy $\|s(0)\|_\infty < \sigma$.

Proposition 3 (Approach to the residual set). *Under the conditions of Proposition 2, define*

$$\begin{aligned} z_i(t) &= \max\{|s_i(t)| - r_b, 0\}, \\ V_s(t) &= \frac{1}{2}\sum_{i=1}^{3} z_i(t)^2, \qquad a_s = \frac{\Xi + \eta}{\sigma - r_b} > 0. \end{aligned} \tag{34}$$

Then

$$z_i(t) \le z_i(0)e^{-a_s t}, \qquad V_s(t) \le V_s(0)e^{-2a_s t}. \tag{35}$$

For every $0 < \delta_s < \sigma - r_b$, a sufficient entrance time into the enlarged residual set is

$$T_s(\delta_s) = \frac{1}{a_s}\ln\left(\max\left\{1, \frac{\max_i z_i(0)}{\delta_s}\right\}\right). \tag{36}$$

In particular, $|s_i(t)| \le r_b + \delta_s < \sigma$ for all $t \ge T_s(\delta_s)$.

Proof. Whenever $z_i > 0$, one has $r_i = |s_i| > r_b$. The radial inequality in the proof of Proposition 2 gives

$$\dot{z}_i = \dot{r}_i \le -\frac{(\Xi + \eta)z_i}{\sigma - r_i} \le -\frac{\Xi + \eta}{\sigma - r_b} z_i = -a_s z_i.$$

The positive-part chain rule extends this inequality almost everywhere to $z_i = 0$. Therefore,

$$\dot{V}_s = \sum_{i=1}^{3} z_i \dot{z}_i \le -a_s \sum_{i=1}^{3} z_i^2 = -2a_s V_s. \tag{37}$$

Scalar comparison yields (35), from which (36) follows. For the prescribed initialization $s(0) = 0$, all $z_i(0)$ vanish, and $|s_i(t)| \le r_b$ holds from the initial time. □

The sliding-variable estimates also give explicit tracking-error bounds. From (10) and the definition of s,

$$\dot{e}_1 + ce_1 = s + s_c, \qquad e_2 = s + s_c - ce_1. \tag{38}$$

For $s_c(t) = \bar{s}(0)e^{-\gamma t}$, $s(0) = 0$, and $c \ne \gamma$, integration gives

$$e_1(t) = e^{-ct}e_1(0) + \int_0^t e^{-c(t-\tau)}s(\tau)\,d\tau + \bar{s}(0)\frac{e^{-\gamma t} - e^{-ct}}{c - \gamma}.$$

Let $S_0 = \|\bar{s}(0)\|_\infty$. Since $|s_i(t)| \le r_b$,

$$\begin{aligned} \|e_1(t)\|_\infty \le e^{-ct}\|e_1(0)\|_\infty + \frac{r_b}{c}(1 - e^{-ct}) \\ + S_0\frac{|e^{-\gamma t} - e^{-ct}|}{|c - \gamma|}. \end{aligned} \tag{39}$$

Define

$$m_e = \min\{c, \gamma\} > 0, \qquad A_e = \|e_1(0)\|_\infty + \frac{S_0}{|c - \gamma|}.$$

Equations (38) and (39) imply the uniform estimates

$$\begin{aligned} \|e_1(t)\|_\infty &\le \frac{r_b}{c} + A_e e^{-m_e t}, \\ \|e_2(t)\|_\infty &\le 2r_b + (cA_e + S_0)e^{-m_e t}. \end{aligned} \tag{40}$$

In particular,

$$\limsup_{t\to\infty} \|e_1(t)\|_\infty \le \frac{r_b}{c}, \qquad \limsup_{t\to\infty} \|e_2(t)\|_\infty \le 2r_b.$$

For any prescribed margins $\delta_1, \delta_2 > 0$, define

$$T_e = \frac{1}{m_e} \ln\left(\max\left\{ 1, \frac{A_e}{\delta_1}, \frac{cA_e + S_0}{\delta_2} \right\} \right). \tag{41}$$

Then, for all $t \ge T_e$,

$$\|e_1(t)\|_\infty \le \frac{r_b}{c} + \delta_1, \qquad \|e_2(t)\|_\infty \le 2r_b + \delta_2.$$

These estimates establish finite-time entrance into prescribed enlargements of the ultimate tracking-error bounds. Together with the bounded reference trajectory, (40) supplies a bounded enclosure for x_1 and x_2. The approximation domain $\mathcal{X}$ is required to contain this enclosure so that the assumed approximation bounds remain applicable.

5. Simulation Analysis

5.1. Simulation Setup and Internal Signals

Numerical simulations are performed in MATLAB/Simulink for the roll, pitch, and yaw attitude channels. The nominal quadrotor parameters are listed in Table 1. The nonlinear uncertainties are specified as $f_1(X) = -0.8\dot{p}$, $f_2(X) = -0.8\dot{q}$, and $f_3(X) = -0.8\dot{r}$, and the external disturbances are $d_i(t) = 0.05\sin(t)$, $i = 1, 2, 3$. A matched actuator fault is introduced at $t_f = 6$ s according to

$$\rho(x,t) = -0.1\sin(x_1 + x_2)\sin(0.1t), \qquad t \ge 6 \text{ s}, \tag{42}$$

and $\rho(x,t) = 0$ for $t < 6$ s. A componentwise torque limit of ± 0.8 N·m is imposed in all controller comparisons. Unless otherwise stated, the plant, reference commands, initial conditions, disturbance, and fault profile are identical for all methods.

Table 1. Nominal physical parameters of the quadrotor.

Parameter	Description	Value
m	Mass	1.121 kg
I_x	Roll moment of inertia	0.0100 kg · m^2
I_y	Pitch moment of inertia	0.0082 kg · m^2
I_z	Yaw moment of inertia	0.0148 kg · m^2
g	Gravitational acceleration	9.8 m/s^2

The observer parameters are selected as $\hat{\varepsilon} = 0.01$, $L = 0.1$, $\beta = 0.5$, $p = 1$, and $q = 3$, where $L = 0.1$ satisfies the positive-gain condition in Proposition 1. The modified sliding-surface and barrier-gain parameters are $c = 5$, $\gamma = 3.4$, $\eta = 1$, and $\sigma = 0.005$. The reference and simulated attitude trajectories remain within the moderate-angle, nonsingular operating domain specified in Assumption 1.

Figure 2 shows the sliding variables of the proposed controller. The choice $s_c(0) = \bar{s}(0)$ gives $s(0) = 0$. After the initial transient and the fault occurrence at $t = 6$ s, all three sliding variables remain inside the prescribed domain, in agreement with the forward-invariance property established in Proposition 2.

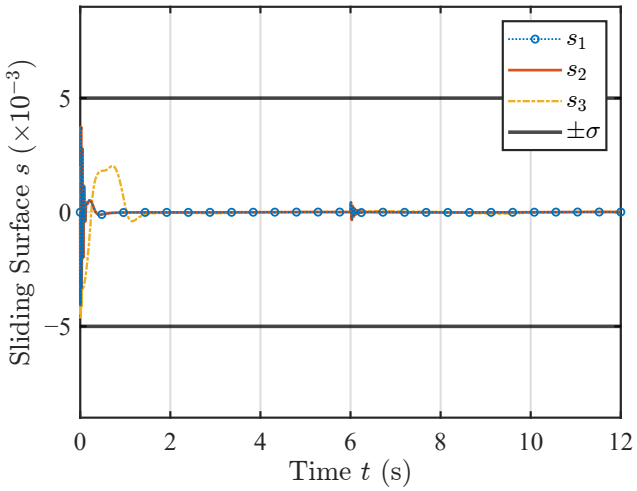


Figure 2. Sliding variables of the proposed controller.

Figure 3 compares the lumped nominal uncertainty P with its RBFNN estimate $\hat{P}$. Following a short initial transient, $\hat{P}$ closely follows the variation of P, demonstrating the online approximation capability of the observer. The remaining approximation error is compensated by the robust term in the control law.

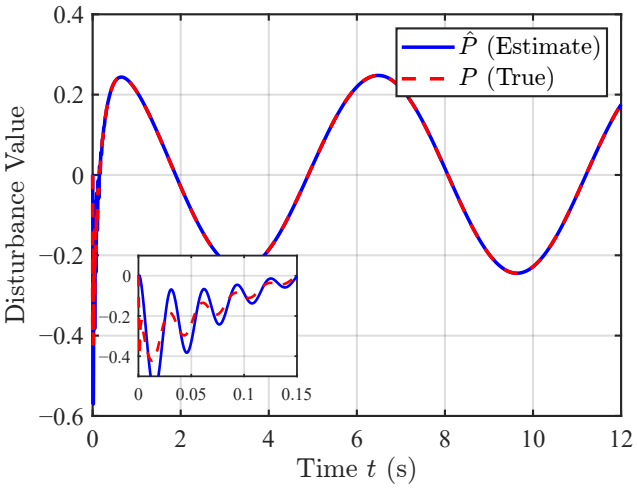


Figure 3. RBFNN approximation of the nominal nonlinear uncertainty and external disturbance.

5.2. Comparison with an External ABFTSMC Benchmark

The proposed controller is compared with the adaptive barrier fast terminal sliding-mode actuator-fault-tolerant controller (ABFTSMC) reported in [37]. The attitude-loop parameters are set to $b_1 = b_2 = 9$, $\alpha = 2$, $\beta = 3$, $\mu = 5$, $\rho = 5$, and $\zeta = 1$, and the attitude switching times are $[2.1, 1.4, 1.38]$ s, as reported in [37]. The additional numerical regularization quantities required for implementation are set to 0.02 for the barrier neighborhood, 0.05 rad/s for the zero-velocity regularization, and 0.05 for the barrier-denominator margin. Both controllers are evaluated using the same plant, reference, initial state, fault profile, and torque limit, and the parameters of the proposed controller remain unchanged.

For N_f sampled instants in the post-fault interval, the reported error indices are defined over all three attitude channels as

$$\begin{aligned} \mathrm{MAE}_{\mathrm{pf}} &= \frac{1}{3N_f} \sum_{k=1}^{N_f} \sum_{i=1}^{3} |e_i(t_k)|, \\ e_{\max,\mathrm{pf}} &= \max_{i,k} |e_i(t_k)|. \end{aligned} \tag{43}$$

Figures 4–6 present the attitude trajectories, tracking errors, and control torques obtained with the two controllers.

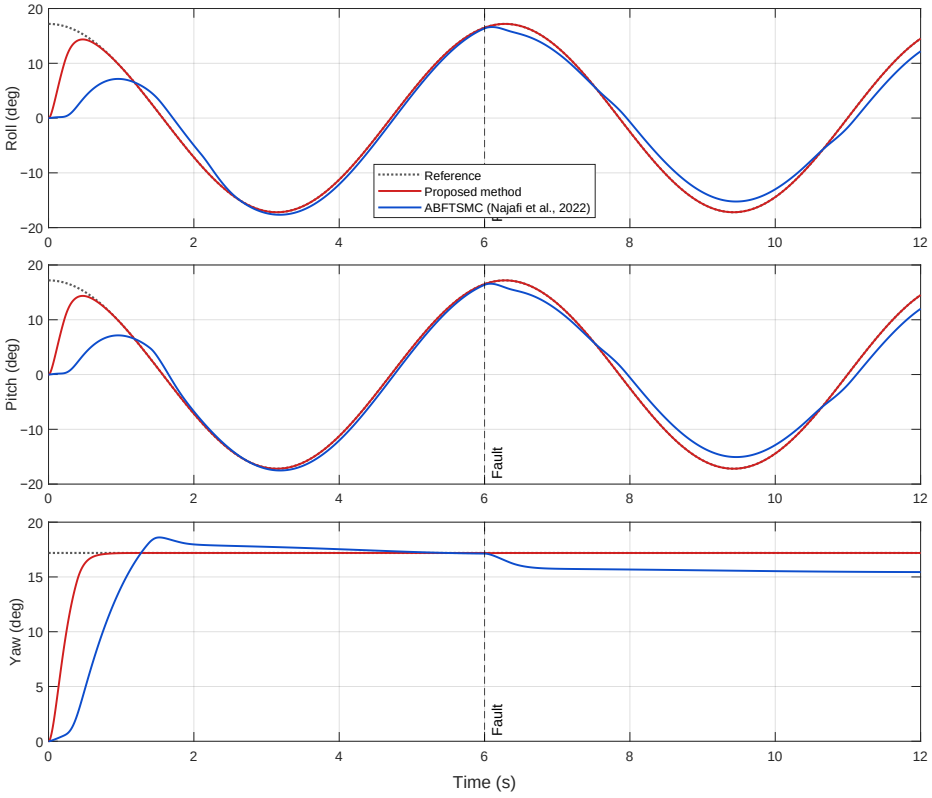


Figure 4. Attitude-tracking comparison with the external ABFTSMC benchmark [37].

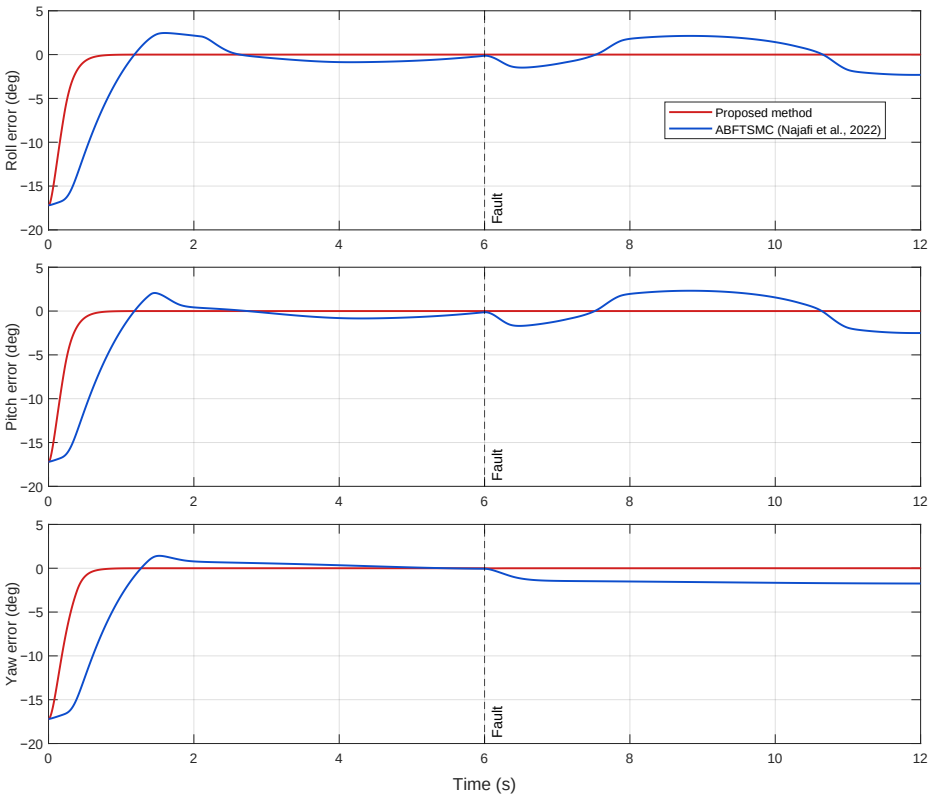


Figure 5. Attitude-error comparison with the external ABFTSMC benchmark [37].

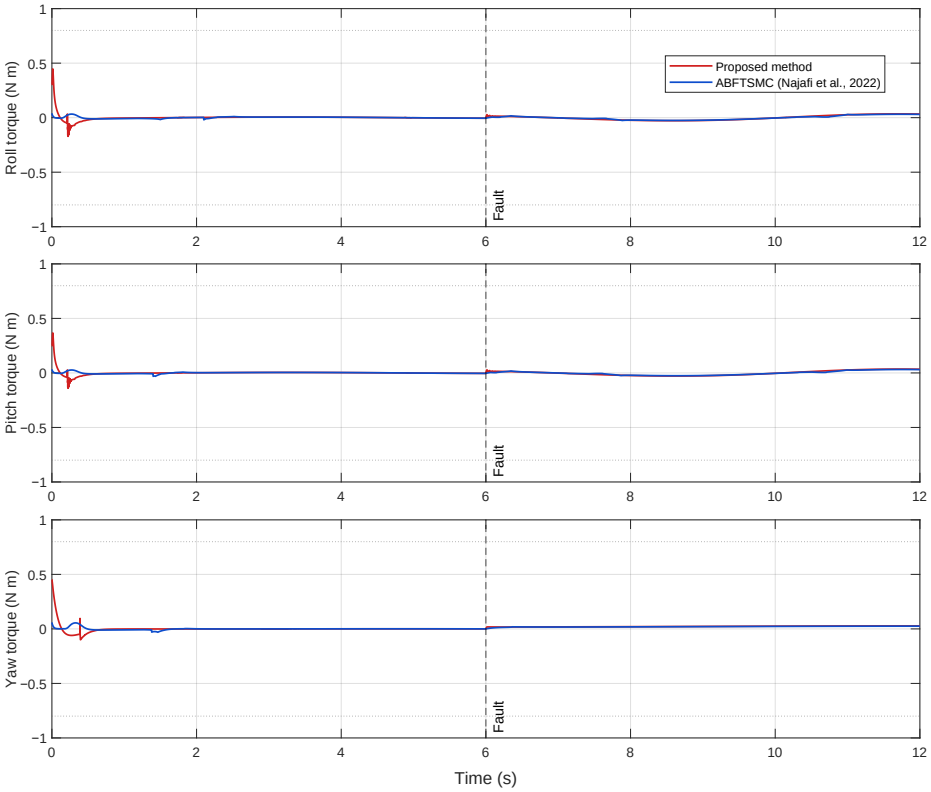


Figure 6. Control-torque comparison with the external ABFTSMC benchmark [37].

Figures 4 and 5 show that the proposed controller suppresses the initial tracking error more rapidly and maintains the roll, pitch, and yaw errors close to zero after the fault is introduced. The ABFTSMC response remains bounded, but exhibits slower convergence and larger post-fault deviations. As shown in Figure 6, the proposed controller generates a stronger transient control action during initial convergence, while the torque in every channel remains below the prescribed 0.8 N·m limit. The results therefore demonstrate improved transient and post-fault tracking performance under the common actuator constraint.

5.3. Combined-Stress Validation

The robustness of the two controllers is further evaluated under simultaneous inertia mismatch, increased disturbance, rate-measurement noise, and the original actuator fault. The multiplicative inertia factors are $[1.20, 0.85, 1.25]$, the disturbance amplitude is increased from 0.05 to 0.15, and band-limited rate noise with a standard deviation of 0.10 deg/s is added. To maintain feasible actuator operation during the initial transient, the initial tracking-error vector is set to $[2.5301, -33.470, -6.4699]^\circ$. The same initial condition is applied to both controllers, the persistent stress levels remain unchanged throughout the simulation, and no controller parameter is retuned.

Figure 7 shows the attitude errors under the combined-stress condition. The proposed controller rapidly attenuates the initial errors and maintains small roll, pitch, and yaw errors following the fault, whereas the ABFTSMC response exhibits larger deviations. Table 2 quantifies the influence of the added stresses on the proposed controller. Relative to the nominal condition, the post-fault MAE and maximum error increase to 0.034895° and 0.125565°, respectively, and the peak torque increases to 0.584273 N·m. The torque remains below the 0.8 N·m limit, confirming that the proposed controller preserves fault-tracking performance without actuator saturation under the specified combination of uncertainties and measurement noise.

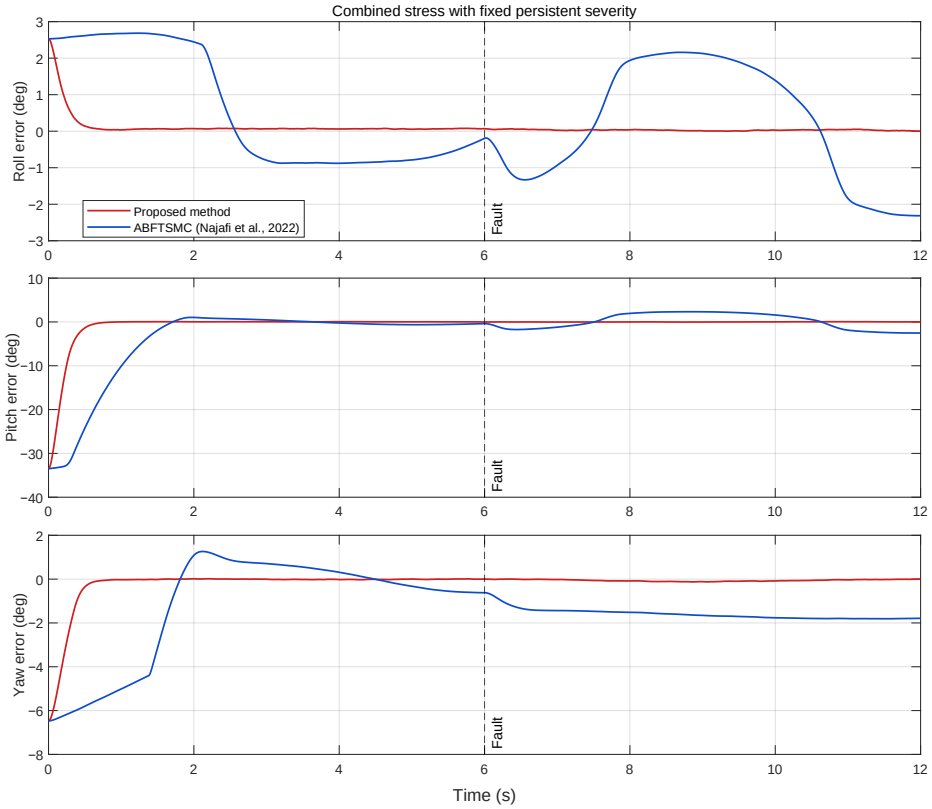


Figure 7. Attitude-error comparison under combined inertia mismatch, disturbance, measurement noise, and the original actuator fault; the ABFTSMC benchmark is from [37].

Table 2. Effect of combined stress on the proposed controller.

Operating Condition	Post-Fault MAE (deg)	Maximum Post-Fault Error (deg)	Peak Torque (N·m)
Nominal condition	0.000953	0.010856	0.452880
Combined-stress condition	0.034895	0.125565	0.584273

5.4. Mechanism-Specific Ablation Study

Two ablation tests are performed to examine the contributions of the modified sliding surface and the RBFNN observer. In the first test, the modified global sliding surface is replaced by a conventional surface over $0 \leq t \leq 4$ s, while the observer, barrier gain, plant, and remaining controller parameters are kept unchanged. The initial attitude is zero and the reference command gives an initial tracking-error vector of $[-17.1887, -17.1887, -17.1887]^\circ$. In the second test, the complete controller is compared with a configuration in which observer compensation is removed. The original actuator fault is introduced at $t = 6$ s, and both configurations use the nominal inertia, nominal disturbance, zero measurement noise, and identical initial conditions.

Figure 8 compares the initial transients produced by the two sliding surfaces. Starting from the same tracking error, the modified global surface drives all three attitude errors rapidly toward zero, whereas the conventional surface exhibits a much slower decay over the same interval. This result demonstrates the contribution of the modified surface to the initial convergence response.

Figure 9 compares the post-fault responses with and without observer compensation. The complete controller confines the three attitude errors to a narrow neighborhood of zero after the fault, while removing the observer produces larger low-frequency deviations in

the roll and pitch channels and a persistent yaw error. The comparison confirms that online observer compensation improves the post-fault tracking response.

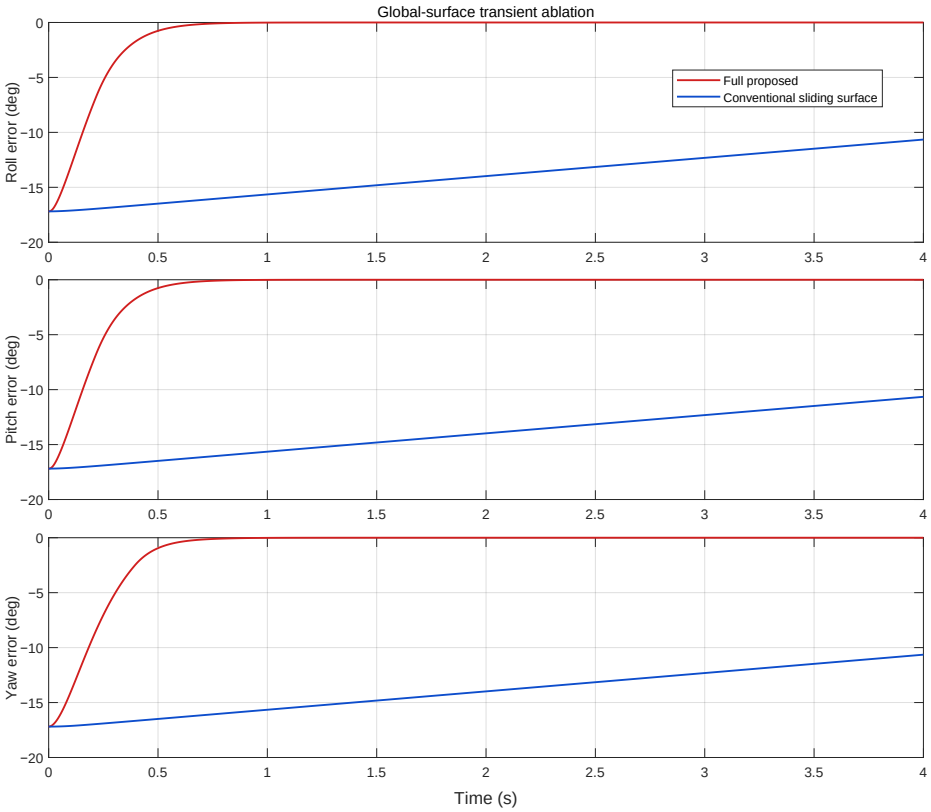


Figure 8. Pre-fault error comparison for the modified global and conventional sliding surfaces.

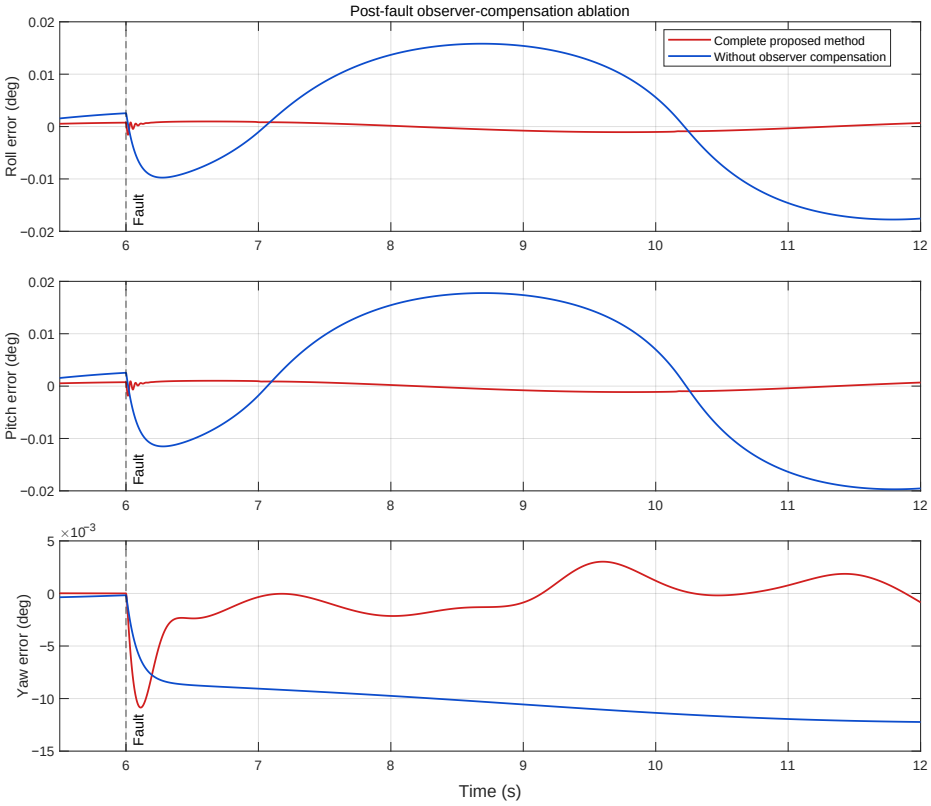


Figure 9. Post-fault error comparison with and without observer compensation.

https://doi.org/10.3390/act15110611

Taken together, the comparative and ablation results demonstrate that the proposed controller provides rapid attitude-error attenuation, maintains bounded control torques under the nominal and combined-stress conditions, and benefits from both the modified sliding surface and the RBFNN observer.

6. Conclusions

This study developed an observer-assisted barrier adaptive sliding mode controller for fault-tolerant quadrotor attitude tracking. Under the stated approximation and fault bounds, the analysis establishes finite-time entry of the observer error into an explicit neighborhood, forward invariance of the prescribed sliding domain, and bounded barrier gains and tracking errors. The comparative simulations show improved post-fault accuracy relative to the ABFTSMC benchmark while keeping the simulated control torques within their prescribed limits. The ablation results further indicate that the modified sliding surface primarily improves the initial transient, whereas observer compensation enhances the post-fault response. These results support the proposed division of compensation tasks between the observer and the barrier term. Future work will address explicit actuator-constrained synthesis and hardware flight validation.

Author Contributions: Conceptualization, D.A. and C.Z.; methodology, C.Z.; software, C.Z.; validation, D.A., C.Z. and F.L.; formal analysis, C.Z.; investigation, C.Z.; resources, D.A.; data curation, F.L.; writing—original draft preparation, C.Z.; writing—review and editing, D.A. and F.L.; visualization, C.Z.; supervision, D.A.; project administration, D.A.; funding acquisition, D.A. All authors have read and agreed to the published version of the manuscript.

Funding: This research was funded by the National Natural Science Foundation of China, grant numbers 61004012, 62371013, and U24A20267.

Institutional Review Board Statement: Not applicable.

Informed Consent Statement: Not applicable.

Data Availability Statement: The data that support the findings of this study are available from the corresponding author upon reasonable request.

Conflicts of Interest: The authors declare no conflicts of interest.

References

1. Hassanalian, M.; Abdelkefi, A. Classifications, applications, and design challenges of drones: A review. *Prog. Aerosp. Sci.* **2017**, *91*, 99–131.
2. Lhayani, M.; Abbou, A.; Houm, Y.E.; Mahmoudi, H. Adaptive nonsingular fast terminal sliding mode control based finite-time disturbance observer for a quadrotor system. *Proc. Inst. Mech. Eng. Part I J. Syst. Control Eng.* **2025**, *239*, 761–789.
3. Mahmood, A.; Ur Rehman, F.; Okasha, M.; Saeed, A. Neural adaptive sliding mode control for camera positioner quadrotor UAV. *Int. J. Aeronaut. Space Sci.* **2025**, *26*, 733–747.
4. Ali, S.; Samar, R.; Shah, M.; Bhatti, A.I.; Munawar, K.; Al-Sggaf, U.M. Lateral guidance and control of UAVs using second-order sliding modes. *Aerosp. Sci. Technol.* **2016**, *49*, 88–100.
5. Yang, P.; Xuan, Y.; Li, W. Adaptive Nonsingular Fast-Reaching Terminal Sliding Mode Control Based on Observer for Aerial Robots. *Actuators* **2024**, *13*, 98. https://doi.org/10.3390/act13030098.
6. Razmi, H.; Afshinfar, S. Neural network-based adaptive sliding mode control design for position and attitude control of a quadrotor UAV. *Aerosp. Sci. Technol.* **2019**, *91*, 12–27.
7. Han, X.; Wang, H.; Hui, N.; Yue, G. Research on Hierarchical Composite Adaptive Sliding Mode Control for Position and Attitude of Hexarotor UAVs. *Actuators* **2025**, *14*, 401. https://doi.org/10.3390/act14080401.
8. Wang, T.; Xia, Y.; Zhao, K.; Wei, M.; Luo, W. Finite-time active disturbance rejection control scheme for quadrotor attitude tracking. *ISA Trans.* **2025**, *166*, 325–336.
9. Di, W.; Li, Z.; Lv, D.; Gao, C.; Yang, Y.; Zhou, X. Adaptive finite time fault tolerant control for the quadrotor unmanned aerial vehicles based on time-triggered strategy. *Optim. Control Appl. Methods* **2023**, *44*, 66–80.

10. Tu, W.; Dong, J. Robust sliding mode control for a class of nonlinear systems through dual-layer sliding mode scheme. *J. Frankl. Inst.* **2023**, *360*, 10227–10250.
11. Afifa, R.; Ali, S.; Pervaiz, M.; Iqbal, J. Adaptive backstepping integral sliding mode control of a mimo separately excited DC motor. *Robotics* **2023**, *12*, 105.
12. Song, C.; Ma, X.; Luo, Y.; Yuan, C.; Gao, F.; Huang, J. Ultra-Local Model-Based Finite-Time Sliding Mode Control Using Neural Network Observer for Quadrotor Position and Attitude. *Actuators* **2026**, *15*, 470. https://doi.org/10.3390/act15090470.
13. Almakhles, D.J. Robust backstepping sliding mode control for a quadrotor trajectory tracking application. *IEEE Access* **2020**, *8*, 5515–5525.
14. Labbadi, M.; Cherkaoui, M. Adaptive fractional-order nonsingular fast terminal sliding mode based robust tracking control of quadrotor UAV with Gaussian random disturbances and uncertainties. *IEEE Trans. Aerosp. Electron. Syst.* **2021**, *57*, 2265–2277.
15. Tian, D.; Xu, R.; Sariyildiz, E.; Gao, H. An adaptive switching-gain sliding-mode-assisted disturbance observer for high-precision servo control. *IEEE Trans. Ind. Electron.* **2021**, *69*, 1762–1772.
16. Mien, V.; Ge, S.S. Adaptive fuzzy integral sliding mode control for robust fault tolerant control of robot manipulators with disturbance observer. *IEEE Trans. Fuzzy Syst.* **2020**, *29*, 1284–1296.
17. Baek, J.; Kang, M. A synthesized sliding-mode control for attitude trajectory tracking of quadrotor UAV systems. *IEEE/ASME Trans. Mechatron.* **2023**, *28*, 2189–2199.
18. Bi, H.; Zou, T.; Zhu, J.; Liu, J. Adaptive super-twisting nonsingular fast terminal sliding mode fault tolerant control of a 2-DOF helicopter with input quantization. *ISA Trans.* **2025**, *160*, 175–185.
19. Yang, P.; Liu, P.; Geng, H.; Jiang, B.; Wen, C. Barrier function based adaptive global sliding mode fault-tolerant control of quadrotor UAV. *Int. J. Control Autom. Syst.* **2023**, *21*, 800–809.
20. Zhang, C.; Wang, J.; Fan, S. Adaptive sliding-mode anti-disturbance attitude control for UAVs with actuator faults and dead zones. *Int. J. Robust Nonlinear Control* **2026**, *36*, 2273–2286.
21. Miao, H.; Song, T.; Liu, J.; Ye, J. Adaptive disturbance observer-based fast nonsingular terminal sliding mode control for quadrotors. *J. Frankl. Inst.* **2024**, *361*, 107092.
22. Li, P.; Yang, H.; Han, Q.; Jin, R. Nonlinear ESO-based surrounding control of quadrotors for a ground moving target. *Robot. Auton. Syst.* **2026**, *203*, 105529.
23. Cao, T.; Guo, B.; Chen, Z.; Yang, S. Learning observer-based sliding mode control for high-order helicopter with uncertainties and disturbances. *Aircr. Eng. Aerosp. Technol.* **2026**, *98*, 49–61.
24. Xu, L.; Qin, K.; Tang, F.; Shi, M.; Lin, B. A novel attitude control strategy for a quadrotor drone with actuator dynamics based on a high-order sliding mode disturbance observer. *Drones* **2024**, *8*, 131.
25. Wang, Z.; Shao, S.; Zhao, Y. Prescribed-time unknown input observer-based UAV attitude tracking control with uncertainties. In Proceedings of the 2024 36th Chinese Control and Decision Conference (CCDC), Xi'an, China, 25–27 May 2024; pp. 6078–6083.
26. Shang, Y.; Cai, G.; Bu, X.; Mu, C.; Wu, T.; Xu, H. Prescribed performance sliding mode synchronization of chaotic systems via neural network-based disturbance observer. *Commun. Nonlinear Sci. Numer. Simul.* **2026**, *157*, 109753. https://doi.org/10.1016/j.cnsns.2026.109753.
27. Wang, L.; Liu, J.; Cao, R.; Yuan, D. Adaptive Fixed-Time Active Fault-Tolerant Control for Nonlinear Systems Based on Super-Twist Sliding Mode and RBFNN. *IET Control Theory Appl.* **2025**, *19*, e70078.
28. Shao, X.; Zhang, F.; Liu, J.; Zhang, Q. Finite-time learning-based optimal elliptical encircling control for UAVs with prescribed constraints. *IEEE Trans. Intell. Transp. Syst.* **2025**, *26*, 7065–7080. https://doi.org/10.1109/TITS.2025.3549827.
29. Mei, Z.; Shao, X.; Xia, Y.; Liu, J. Enhanced fixed-time collision-free elliptical circumnavigation coordination for UAVs. *IEEE Trans. Aerosp. Electron. Syst.* **2024**, *60*, 4257–4270. https://doi.org/10.1109/TAES.2024.3374708.
30. Li, S.; Shao, X.; Wang, H.; Liu, J.; Zhang, Q. Adaptive critic attitude learning control for hypersonic morphing vehicles without backstepping. *IEEE Trans. Aerosp. Electron. Syst.* **2025**, *61*, 8787–8803. https://doi.org/10.1109/TAES.2025.3542345.
31. Cheng, Y.; Shao, X.; Li, J.; Liu, J.; Zhang, Q. Concurrent learning-based adaptive critic formation for multirobots under safety constraints. *IEEE Internet Things J.* **2025**, *12*, 7610–7621. https://doi.org/10.1109/JIOT.2024.3497979.
32. Yang, W.; Cui, G.; Ma, Q.; Ma, J.; Tao, C. Finite-time adaptive event-triggered command filtered backstepping control for a QUAV. *Appl. Math. Comput.* **2022**, *423*, 126898.
33. Liu, K.; Wang, X.; Wang, R.; Sun, G.; Wang, X. Antisaturation finite-time attitude tracking control based observer for a quadrotor. *IEEE Trans. Circuits Syst. II Express Briefs* **2020**, *68*, 2047–2051.
34. Ge, S.S.; Wang, C. Adaptive neural control of uncertain MIMO nonlinear systems. *IEEE Trans. Neural Netw.* **2004**, *15*, 674–692.
35. Wang, H.; Liu, P.X.; Zhao, X.; Liu, X. Adaptive fuzzy finite-time control of nonlinear systems with actuator faults. *IEEE Trans. Cybern.* **2020**, *50*, 1786–1797.

36. Ding, S.; Li, K.X.; Li, S. Robust finite-time tracking control for a class of nonlinear systems via fractional sliding mode. *IEEE Trans. Ind. Electron.* **2015**, *62*, 4905–4912.
37. Najafi, A.; Vu, M.T.; Mobayen, S.; Asad, J.H.; Fekih, A. Adaptive barrier fast terminal sliding mode actuator fault tolerant control approach for quadrotor UAVs. *Mathematics* **2022**, *10*, 3009. https://doi.org/10.3390/math10163009.

Disclaimer/Publisher's Note: The statements, opinions and data contained in all publications are solely those of the individual author(s) and contributor(s) and not of MDPI and/or the editor(s). MDPI and/or the editor(s) disclaim responsibility for any injury to people or property resulting from any ideas, methods, instructions or products referred to in the content.